Effects of present-day deglaciation in Iceland on mantle melt production rates

P. Schmidt,[1] B. Lund,[1] C. Hieronymus,[1] J. Maclennan,[2] T. Árnadóttir,[3] and C. Pagli[4]

[1] Ongoing deglaciation in Iceland not only causes uplift at the surface but also increases magma production at depth due to decompression of the mantle. Here we study glacially induced decompression melting using 3-D models of glacial isostatic adjustment in Iceland since 1890. We find that the mean glacially induced pressure rate of change in the mantle increases melt production rates by 100–135%, or an additional 0.21–0.23 km^3 of magma per year beneath Iceland. Approximately 50% of this melt is produced underneath central Iceland. The greatest volumetric increase is found directly beneath Iceland's largest ice cap, Vatnajökull, colocated with the most productive volcanoes. Our models of the effect of deglaciation on mantle melting predict a significantly larger volumetric response than previous models which only considered the effect of deglaciation of Vatnajökull, and only mantle melting directly below Vatnajökull. Although the ongoing deglaciation significantly increases the melt production rate, the increase in melt supply rate at the base of the lithosphere is delayed and depends on the melt ascent velocity through the mantle. Assuming that 25% of the melt reaches the surface, the upper limit on our deglaciation-induced melt estimates for central Iceland would be equivalent to an eruption the size of the 2010 Eyjafjallajökull summit eruption every seventh year.

Citation: Schmidt, P., B. Lund, C. Hieronymus, J. Maclennan, T. Árnadóttir, and C. Pagli (2013), Effects of present-day deglaciation in Iceland on mantle melt production rates, *J. Geophys. Res. Solid Earth*, *118*, 3366–3379, doi:10.1002/jgrb.50273.

1. Introduction

[2] The general warming trend during the last century has caused significant thinning of glaciers in Iceland. The largest ice cap, Vatnajökull, is estimated to have lost 435 km^3 of ice during 1890–2004 [*Pagli et al.*, 2007a]. As a consequence, Iceland is currently undergoing glacial isostatic adjustment (GIA) with uplift rates of up to 25–29 mm/yr [*Árnadóttir et al.*, 2009; *Auriac et al.*, 2013]. GIA is, however, not restricted to surface deformation. Glacial unloading causes decompression of the upper mantle, leading to increased generation of magma [e.g., *Harðarson and Fitton*, 1991; *Jull and McKenzie*, 1996; *Pagli and Sigmundsson*, 2008]. In the crust, the changing stress state also affects magma emplacement [e.g., *Hooper et al.*, 2011] and the stability of magma chambers [e.g., *Albino et al.*, 2010].

[3] Decompression melting can occur in the uppermost mantle as the gradient of the solidus temperature (4.3 K/km) [*Katz et al.*, 2003] is steeper than the adiabatic geotherm (0.6 K/km) [*McKenzie and Bickle*, 1988]. A rising parcel of mantle material will therefore be brought closer to its solidus temperature. Depending on the initial temperature and final depth of the parcel, partial melting may initiate. Decompression melting of the mantle can also occur if the in situ pressure decreases. In this case, melting will occur if the solidus temperature is shifted to, or below, the mantle temperature. Conversely, melting in the mantle can be inhibited if the in situ pressure increases. Temporal pressure changes in the mantle, such as GIA, can therefore cause significant variations in the melt production rate [e.g., *Jull and McKenzie*, 1996]. Iceland is an exceptional location where this process can be studied in detail as the island is located on top of a mantle plume, cut through by the Mid-Atlantic Ridge (MAR), and is currently undergoing mantle decompression due to glacial unloading.

[4] In this study we investigate the increase in mantle melting beneath Iceland induced by deglaciation since 1890. We present a detailed view of mantle decompression in both time and space and define a 3-D melting region following the plate boundary across the entire country, as GIA affects all of Iceland. This is a significant development from previous studies which only considered the region under Vatnajökull [e.g., *Pagli and Sigmundsson*, 2008] and therefore did not report on the full impact of current deglaciation on melt production. To convert GIA decompression rates to

---

[1]Department of Earth Sciences, Uppsala University, Uppsala, Sweden.
[2]Department of Earth Sciences, University of Cambridge, Cambridge, UK.
[3]Nordic Volcanological Center, Institute of Earth Sciences, University of Iceland, Reykjavík, Iceland.
[4]School of Earth and Environment, University of Leeds, Leeds, UK.

Corresponding author: P. Schmidt, Department of Earth Sciences, Uppsala University, Villavägen 16, SE-752 36 Uppsala, Sweden. (peter.schmidt@geo.uu.se)
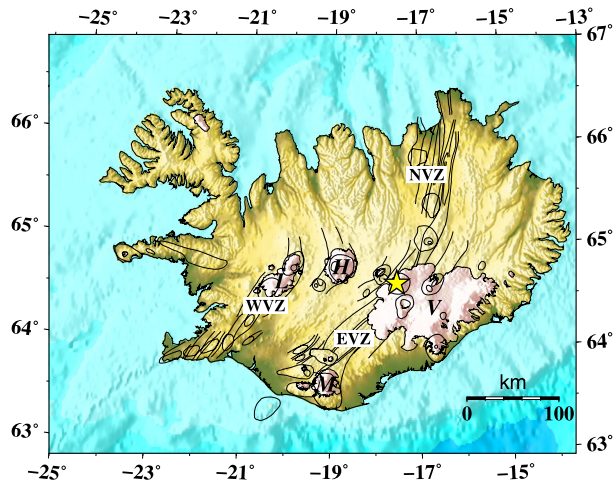
Figure 1. Map of Iceland showing the larger glaciers (white-filled polygons) (L—Langjökull; H—Hofsjökull; M—Mýrdalsjökull; V—Vatnajökull), the approximate location of the plume center (yellow star), central volcanoes and calderas (black ovals), and major features of the rift zones (annotated black lines) mentioned in the text (WVZ— Western Volcanic Zone; EVZ—Eastern Volcanic Zone; NVZ—Northern Volcanic Zone).

melt production rates, we use the melt productivity equation [*McKenzie*, 1984] and a recent melt parametrization, including the effect of water and depletion of clinopyroxene (cpx-out) on mantle melting [*Katz et al.*, 2003]. In this study we also add more detail to previous GIA models of Iceland. The ice history model introduced by *Árnadóttir et al.* [2009] is refined with a more realistic distribution of deglaciation rates on Vatnajökull and the inclusion of a larger number of small glaciers. In addition, we construct a 3-D Earth model with laterally varying elastic thickness derived from the geothermal structure of the Icelandic subsurface [*Kaban et al.*, 2002].

1.1. Iceland

[5] About 11% of the surface of Iceland is currently covered by glaciers [*Björnsson and Pálsson*, 2008]. The island rises above the surrounding seafloor due to the intersection of a mantle plume with the MAR. Since the birth of Iceland, some tens of millions of years ago, the westward drift of the plate boundary with respect to the plume has caused an offset from the general strike of the MAR as the spreading ridge crosses the island (Figure 1). Several rift relocations have created a complex plate boundary across Iceland, with parallel rift zones and oblique spreading in the south [e.g., *Sæmundsson*, 1967; *Hardarson et al.*, 1997, 2008]. Full plate spreading across Iceland is approximately 20 mm/yr [*DeMets et al.*, 1994], and in southern Iceland, spreading is partitioned between the Western Volcanic Zone (WVZ) and the more active Eastern Volcanic Zone (EVZ) [e.g., *LaFemina et al.*, 2005].

[6] Geochemical studies [*Maclennan et al.*, 2001; *Kokfelt et al.*, 2003] indicate that the potential temperature, T_{pot}, varies modestly along the Northern Volcanic Zone (NVZ) ranging from about 1480°C to 1500°C. This is a significantly smaller lateral variation than the estimated

temperature anomaly of the plume conduit (150–200°C) [*Ruedas et al.*, 2007]. The difference is readily interpreted if the plume head is laterally larger and extends deeper than the melting region, in which case T_{pot} is entirely governed by the plume, with relatively small lateral variations. Observations of the plume head using surface wave tomography seem to confirm this scenario [*Allen et al.*, 2002a; *Pilidou et al.*, 2005; *Delorey et al.*, 2007]. The mantle source bulk water content across Iceland and along the MAR is significantly elevated, ranging from 620 to 920 ppm under central Iceland, decreasing to about 165 ppm offshore [*Jamtveit et al.*, 2001; *Nichols et al.*, 2002]. This can be compared to 125 ppm estimated for the mantle source bulk water content beneath a typical mid-ocean ridge [*Hirth and Kohlstedt*, 1996].

[7] Observations of extrusive magma volumes in Iceland show that during and shortly after the late Pleistocene deglaciation some 12,000–10,000 years ago, there was a short pulse of a thirtyfold to fiftyfold increase in the eruption rate [e.g., *Sigvaldason et al.*, 1992; *Maclennan et al.*, 2002]. In addition, the trace element chemistry of late glacial to early postglacial lavas differs from that of glacial or more recent lavas [e.g., *Sigvaldason et al.*, 1992; *Slater et al.*, 1998; *Maclennan et al.*, 2002; *Sinton et al.*, 2005], indicating that deglaciation had a profound influence on volcanism.

1.2. Previous Studies of GIA and the Effect of Deglaciation on Magma Production in Iceland

[8] Present-day GIA in Iceland has been studied and modeled by several authors using measurements of tilt rates, GPS, gravity, and, more recently, interferometric synthetic aperture radar (InSAR) [e.g., *Sigmundsson and Einarsson*, 1992; *Fleming et al.*, 2007; *Pagli et al.*, 2007a; *Jacoby et al.*, 2009; *Árnadóttir et al.*, 2009; *Schmidt et al.*, 2012a; *Auriac et al.*, 2013]. Most of the earlier studies assumed axisymmetric models, considering only the deglaciation of Vatnajökull, and used regional observations to constrain the modeling. The first countrywide study by *Árnadóttir et al.* [2009] showed, however, that the deglaciation of the glaciers Hofsjökull, Langjökull, Mýrdalsjökull, and Eyjafjallajökull has a significant effect on the uplift velocities, in particular, in central Iceland. *Árnadóttir et al.* [2009] used nationwide GPS measurements to constrain the Earth model and found a best fit for an effective thickness of the elastic lithosphere of 40 km and a 10^{19} Pa s viscoelastic mantle. This estimate of mantle viscosity is in agreement with previous estimates from GIA studies as well as with the upper range of estimates from investigations of postseismic and postrifting relaxation [e.g., *Pollitz and Sacks*, 1996; *Hofton and Foulger*, 1996; *LaFemina et al.*, 2005; *Árnadóttir et al.*, 2005].

[9] A link between deglaciation and increased melting beneath Iceland at the end of the last ice age was first suggested by *Harðarson and Fitton* [1991]. They showed that a minor amount of increased melting in the mantle can explain the anomalous trace element chemistry observed in late glacial lavas at the off-ridge volcano Snæfellsjökull. *Jull and McKenzie* [1996] studied the effect of the late Pleistocene deglaciation in Iceland on melt production rates using an axisymmetric GIA model, the melt productivity equation [*McKenzie*, 1984], and a melt parametrization by *McKenzie and Bickle* [1988, MB88 hereinafter]. They found that the
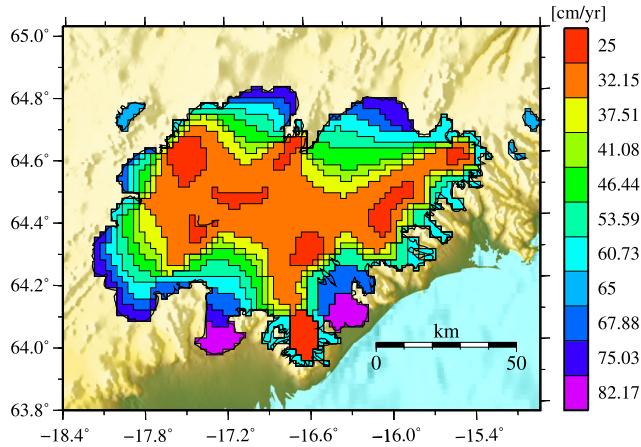
Figure 2. Ice model of Vatnajökull colored by deglaciation rates. The solid black line marks the glacier outline used to set up the ice model. The ice model also includes the smaller glaciers seen on the map, Tungnafellsjökull in the northwest, Þrándarjökull, and Hofsjökull in Lón to the east.

melt production rate in the mantle rose to about 3.5 km^3/yr during deglaciation. Melting due to passive upwelling was estimated to be about 0.12 km^3/yr. During deglaciation, the melt production rates were thus increased by a factor of about 30, in good agreement with observed temporal variations in erupted magma volumes. *Jull and McKenzie* [1996] emphasized that the total melt volume balances over long time scales. During glacier growth, the pressure increases in the mantle, thereby inhibiting melting for the length of time it takes to bring the mantle back to preglacial pressures. As the pressure is released during deglaciation, the additional melt generated balances the previously reduced melt volumes.

[10] The effect of present-day deglaciation on melt production was studied by *Pagli and Sigmundsson* [2008] and *Sigmundsson et al.* [2010]. Decompression rates in the mantle were computed using an axisymmetric Earth model, loaded by the deglaciation of Vatnajökull since 1890, and converted into melt production rates. Following *Jull and McKenzie* [1996], these studies also used the melt productivity equation by *McKenzie* [1984] but combined with a melt parametrization from *McKenzie* [1984, equation D8, M84-D8 hereinafter] instead of the MB88 model. *Pagli and Sigmundsson* [2008] estimated that the present-day increase in the melt production rate in the rift beneath Vatnajökull is about 0.014 km^3/yr.

2. Modeling GIA Pressure Changes in the Mantle

[11] To estimate the amount of glacially induced melting beneath Iceland, we need to know the pressure changes in the mantle induced by the ice mass changes at the surface. For this purpose, we construct a 3-D finite element model consisting of an Earth model loaded by an ice history model, jointly referred to as a GIA model. In this section, we describe the ice history model, investigate suitable Earth models, and study the rate of pressure change in the mantle.

2.1. Ice History Model

[12] The ice history model used here (included as supporting information) builds upon the model developed by *Árnadóttir et al.* [2009], mainly differing by a finer grid (2 × 2 km), a more detailed deglaciation of Vatnajökull, and the inclusion of several smaller glaciers. The volumetric ice loss is based on the estimated volume loss of Vatnajökull of 435 km^3 over the period 1890–2004 [*Pagli et al.*, 2007a] (we note that the estimate of 300 km^3 presented in *Björnsson and Pálsson* [2008] is a misprint and should be 435 km^3 (H. Björnsson, personal communication, 2010)). Assuming a constant deglaciation rate over the period, we extrapolate this value to yield 458 km^3 over the period 1890–2010. Based on the annual net mass balance, b$_n$, between glacier years 1991/1992 and 2005/2006 [Figure 5 in *Björnsson and Pálsson*, 2008], the interior of Vatnajökull is divided into nine regions differing by Δb$_n$ = 1 m water equivalent (mwe) mass loss between adjacent regions (Figure 2). In addition, we subdivide the region between b$_n$ = ±0.5 mwe into two equal-size regions, giving a total of 10 regions. The deglaciation rate of the innermost region is assigned a fixed value of 25 cm/yr while the deglaciation rates of the other regions are increased linearly with b$_n$ (Figure 2).

[13] The ice history model includes the large glaciers Vatnajökull, Hofsjökull, Langjökull, Mýrdalsjökull, and Eyjafjallajökull and several smaller glaciers (Table 1). We assign a constant melting rate of 65 cm/yr to all glaciers except Vatnajökull, similar to the value used by *Árnadóttir et al.* [2009]. We do not include the distant glaciers Drangajökull and Snæfellsjökull, as there is no signal in our GPS data indicating local uplift there.

[14] The assumption of a temporally constant deglaciation rate is crude, as it is well known that the deglaciation rates have varied over the model period, even including periods of growth. It has further been noted that the deglaciation rate has increased in recent years [*Björnsson and Pálsson*, 2008]. Unfortunately, we do not have sufficient observational data on the glaciers to constrain an ice model with time-varying deglaciation rates. We do not model the ice history prior to 1890 since it is less well constrained than the more recent evolution, and the effect of the earlier ice history on present-day displacement rates is small [*Árnadóttir et al.*, 2009; *Fleming et al.*, 2007]. This is mainly due to the volume of the glaciers being relatively constant between the years 1750 and 1890 [*Thórarinsson*, 1943; *Björnsson*, 1979] and the low viscosity of the Icelandic mantle.

Table 1. Summary of the Volumetric Loss in the Ice History Model Between 1890 and 2010[a]

Glacier	Area (km^2)	Deglaciation Rate (cm/yr)	Volume Loss (km^3)
Vatnajökull	8428	25–82.17	458
Langjökull	1024	65	79.9
Hofsjökull	976	65	76.1
Mýrdalsjökull	688	65	53.7
Eyjafjallajökull	96	65	7.5
Smaller glaciers	230	65	17.9
Total	11,442	–	693.1

[a]The "Smaller glaciers" group includes the glaciers Torfajökull, Tindfjallajökull, Eiríksjökull, Þórisjökull, Hrútfell, Tungnafellsjökull, Þrándarjökull, and Hofsjökull in Lón.

[15] The retreat of the ice edge of Vatnajökull, the largest glacier, is on average about 1 km since 1890 (equivalent to 5–10% decrease in area since 1890), with peak values of 2–3 km at some outlet glaciers [*Björnsson*, 1979]. This is on the order of up to 1.5 element widths in the ice model. We therefore neglect fluctuations in the areal extent of the glaciers. We do note, however, that our ice model predicts surface velocities that well match high spatial resolution InSAR data right up to the edge of Vatnajökull [*Auriac et al.*, 2013].

2.2. Earth Model Description

[16] We set up the GIA model in the commercial finite element software Abaqus following the recipe of *Wu* [2004], modified according to *Schmidt et al.* [2012b] to allow for laterally varying material layers. The horizontal element size of the Earth model is 6×6 km down to a depth of 300 km, with an average element thickness of 6 km in the mantle. In the region covered by the glaciers, the horizontal element size is decreased to 2×2 km to match the ice history model. The elastic lithosphere of Iceland is modeled using eight element layers. At depths greater than 670 km and outside the Icelandic coast, the Earth model is expanded to a half sphere of radius $\sim41{,}000$ km and embedded in infinite elements to avoid boundary effects.

[17] The Earth model is specified by five parameters, density, Young's modulus, Poisson's ratio, viscosity (η), and the elastic thickness of the lithosphere (h_e). Test models show that the vertical displacement rates in our models are mainly sensitive to the viscosity and elastic thickness. We therefore constrain the density, Young's modulus, and Poisson's ratio by volume averages of the preliminary reference Earth model [*Dziewonski and Anderson*, 1981], noting that the densities in this model differ somewhat from those inferred for the Icelandic crust [e.g., *Gudmundsson*, 2003]. To constrain h_e and η, we use the uplift rates estimated from two nationwide GPS campaigns in 1993 and 2004, as well as 10 continuous GPS stations [*Árnadóttir et al.*, 2009]. This data set comprises some 125 stations evenly distributed over Iceland. We run a set of 1-D models with uniform elastic thickness and homogeneous mantle viscosity. The fit of the GIA model to the vertical GPS velocities is quantified with the normalized χ_v^2 value:

$$\chi_v^2 = \frac{1}{N-m} \sum_{i=1}^{N} \left(\frac{v_i^{\mathrm{obs}} - v_i^{\mathrm{mod}}}{\sigma_i} \right)^2 \quad (1)$$

where N is the number of observations, m is the number of free parameters in the model, σ_i is the uncertainty of the observations, and v_i^{obs} and v_i^{mod} are the observed and modeled vertical velocities, respectively.

[18] The 1-D Earth model that best fits the GPS data has an elastic thickness of 35 km and a viscosity of 10^{19} Pa s. In general, we find that the viscosity is well constrained while the elastic thickness is less so. We find a weak trade-off between these parameters, with slightly larger preferred viscosity associated with thinner elastic thickness. This is in agreement with the results of *Árnadóttir et al.* [2009].

[19] As Iceland has a complex tectonic setting, with offset rift zones, transform zones, and a mantle plume, it is likely that the elastic thickness probed by GIA displays significant lateral variations. The effect of a laterally varying elastic thickness on GIA in Iceland has, however, not been studied before. We therefore include the first study of such lateral variations in Appendix A. We find that the GPS data used herein are mainly sensitive to the mean elastic thickness beneath the larger glaciers. We use the depth to the 1200°C isotherm beneath Iceland [*Kaban et al.*, 2002] as a proxy for the lateral variation of h_e and scale this by a factor of 0.67 to yield a mean elastic thickness of 35 km beneath the larger glaciers (see Appendix A for more details). This proxy was chosen because h_e constrains the upper boundary in our model of the melting region, which we describe in section 4.1. Including lateral variation in h_e has negligible effect on the decompression rates in the mantle, except in the uppermost few kilometers.

2.3. Rate of Pressure Change in the Mantle

[20] We find the maximum decompression rate in our GIA model, 1450 Pa/yr, just below the elastic lithosphere beneath Vatnajökull (Figure 3c). We note, however, that the depth to the local maximum decompression rate increases with distance from the glaciers, in agreement with the decompression rates presented in *Jull and McKenzie* [1996] and *Sigmundsson et al.* [2010]. Beneath Krafla (Figure 3d), the greatest decompression rate occurs at a depth of 90 km, while below Snæfellsjökull or the northern margin of the Northern Volcanic Zone (Figures 3a and 3e), the decompression rate increases down to a depth of about 210 km. Our estimated maximum decompression rate is comparable to the estimate by *Pagli and Sigmundsson* [2008] of 1700 Pa/yr, whereas *Sigmundsson et al.* [2010] estimate even higher decompression rates. The reason for the lower estimates found here is most likely the spatial distribution of thinning glaciers in the ice history model. As shown by *Sigmundsson et al.* [2010] for the Vatnajökull ice cap, the maximum decompression rate in the mantle will decrease if deglaciation is concentrated toward the edges of the glacier.

[21] Changing the density, Young's modulus, or Poisson's ratio of the mantle has negligible effect on the decompression rate in the sublithospheric mantle, whereas a significant pressure response is observed in the elastic lithosphere. In this paper, we are mainly interested in pressure changes in the sublithospheric mantle and will therefore not discuss the pressure in the elastic lithosphere further. Among the Earth model parameters, the decompression rate in the mantle is mainly sensitive to the mean elastic thickness of the lithosphere and to a lesser extent the mantle viscosity. Increasing the elastic thickness from 10 to 50 km increases the decompression rates by up to 50%, while decreasing the viscosity from 15×10^{18} to 5.5×10^{18} Pa s increases the decompression rate by a maximum of about 30%. However, the sensitivity to the elastic thickness and the viscosity quickly decreases with depth.

[22] The decompression rate is not constant with time. We find that the estimated dP/dt varies by up to 75% over the modeled period (Figures 3f and 3g), as also noted by *Sigmundsson et al.* [2010]. The detailed evolution of the decompression rates reflects a transition from the immediate elastic response at the onset of deglaciation to a viscous response as deglaciation proceeds. This is most evident directly beneath the elastic layer (Figure 3f) but can also be seen at greater depth (Figure 3g). In general, the temporal variation in dP/dt decreases with increasing depth. For
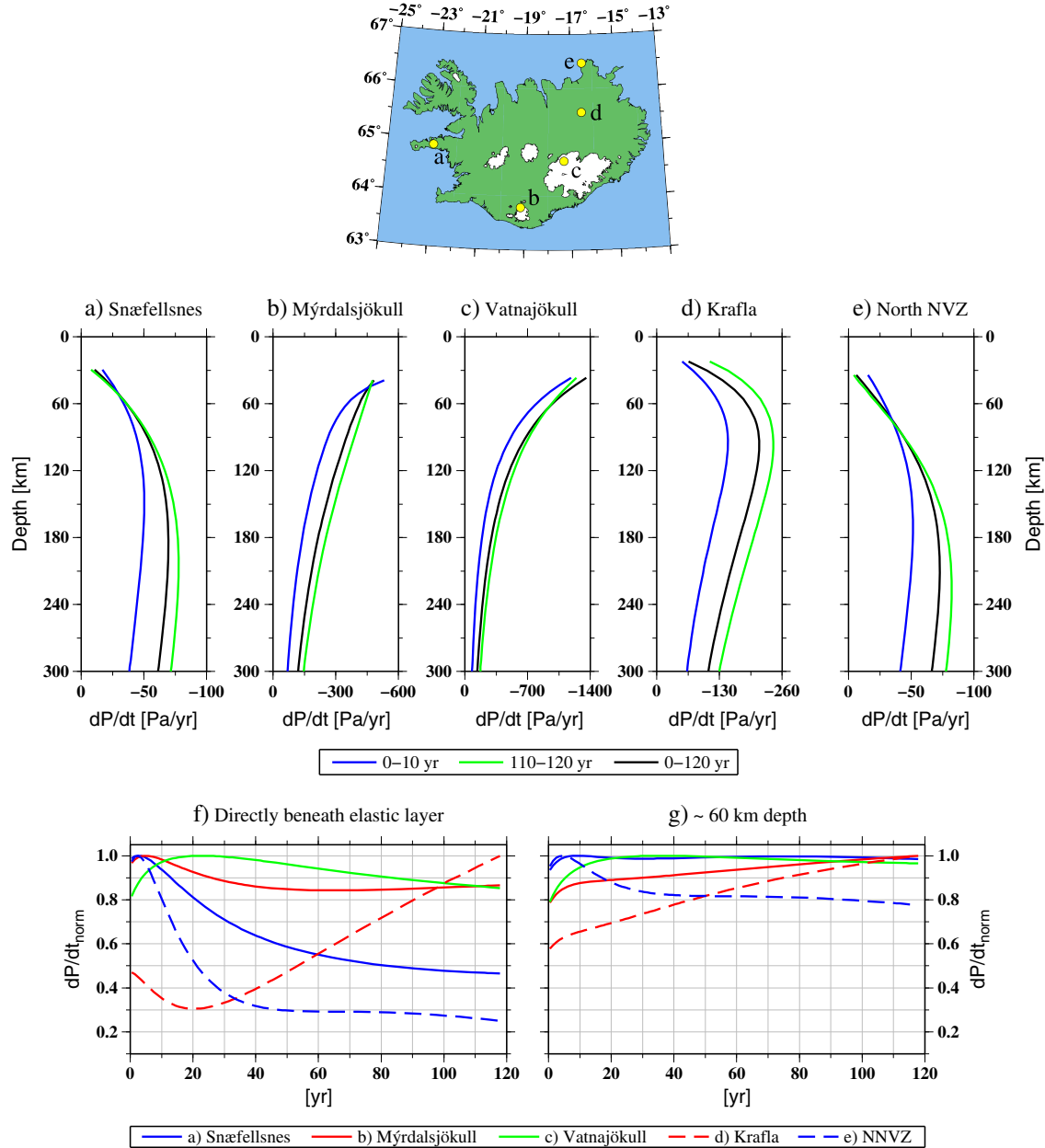
Figure 3. Predicted glacially induced pressure changes (dP/dt) in the mantle as a function of depth and time at selected locations across Iceland. (top) The locations of the depth profiles a–e. (a–e) The dP/dt as a function of depth averaged over the time periods (model years) 0–10 (blue), 110–120 (green), and 0–120 (black). (f, g) The temporal variation of dP/dt over the 120 model years, normalized against the maximum value at each site a–e.

a constant deglaciation rate, we find that the decompression rate eventually decreases with time beneath Vatnajökull and at larger distances from the glacier, while beneath sites at intermediate distances, the decompression rate increases with time (Figure 3f). For the melt estimates, we will therefore use the mean decompression rates over the full 120 year model time, evaluated in each subvolume of our model. The decompression trends discussed here, in combination with the geometry of the melting region (see section 4.1), result in the bulk of glacially induced decompression melting occurring at depth, where the temporal variations in decompression rates are of smaller magnitude.

3. Isentropic Decompression Melting of the Mantle

[23] Here we present the theoretical framework we use to convert the decompression rate to mantle melting, as well as the melt parametrization and melt model parameters. We include a brief comparison with the two melt parametrizations used by previous studies on glacially induced mantle melting in Iceland.

3.1. The Melt Productivity Equation

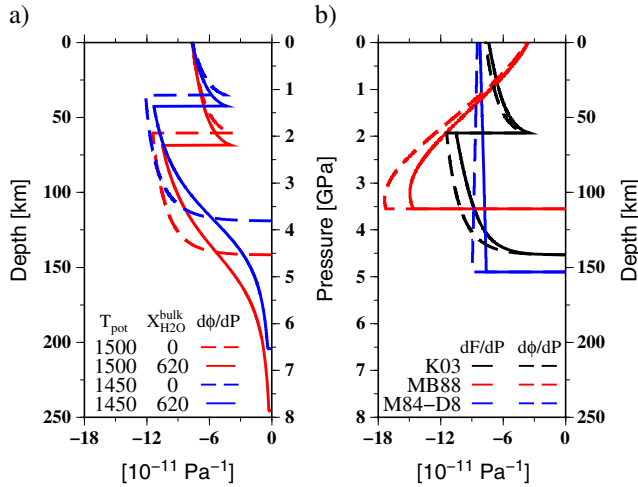[24] The melt productivity equation was initially derived by *McKenzie* [1984] assuming isentropic decompression

a)

b)

Figure 4. (a) Melt productivity by volume, $d\phi/dP$, as a function of pressure and depth for melt parametrization K03 [*Katz et al.*, 2003] and different potential temperatures, T_{pot} (°C), and bulk water contents, $X_{H_2O}^{bulk}$ (ppm). (b) Melt productivity by weight, dF/dP, and by volume, $d\phi/dP$, for the melt parametrizations K03 (dry model), MB88 [*McKenzie and Bickle*, 1988], and M84-D8 [*McKenzie*, 1984, equation D8] for $T_{pot} = 1500$°C. Additional material parameters are listed in Table 3. Depths are based on the assumption of lithostatic pressure and the density stratification given in Table 2.

batch melting

$$\frac{dF}{dP} = \frac{\frac{\alpha^s}{\rho^s} + \left(\frac{\alpha^m}{\rho^m} - \frac{\alpha^s}{\rho^s}\right)F - \frac{(1-F)c_p^s + Fc_p^m}{T}\left(\frac{\partial T}{\partial P}\right)_F}{\Delta s + \frac{(1-F)c_p^s + Fc_p^m}{T}\left(\frac{\partial T}{\partial F}\right)_P} \quad (2)$$

where F is the melt fraction by weight, P is the pressure, T is the temperature, α is the thermal expansion coefficient, ρ is the density, c_p is the specific heat at constant pressure, and Δs is the entropy of fusion. Superscripts s and m refer to the solid and melt, respectively.

[25] The assumption of batch melting can, however, be replaced by assuming thermal equilibrium between the solid residual and the separating melt, as first shown by *Iwamori et al.* [1995]. Various alternative derivations and extensions of the equation have later been presented by several authors [e.g., *Iwamori et al.*, 1995; *Asimow et al.*, 1997; *Phipps Morgan*, 2001; *Rudge et al.*, 2011]. Equation (2) differs from that given by *McKenzie* [1984] in that we allow for different specific heat capacities of the melt and solid phases.

3.2. Mantle Melting Model

[26] To estimate the melt productivity as a function of pressure, we need a description of the relation between F, T, and P in the mantle, after which equation (2) can be integrated with standard methods. Several melt parametrizations based on experimental data can be found in the literature [e.g., *McKenzie*, 1984; *McKenzie and Bickle*, 1988; *Langmuir et al.*, 1992; *Kinzler and Grove*, 1992; *Kinzler*, 1997; *Iwamori et al.*, 1995; *Iwamori*, 1997; *Pertermann and Hirschmann*, 2003]. Here we will use the model by *Katz et al.* [2003, K03 hereinafter], which includes the effect of

the removal of clinopyroxene from the solid (cpx-out), as well as the effect of the bulk water content of the mantle source, $X_{H_2O}^{bulk}$ (Figure 4a). K03 is appropriate for melting of depleted peridotite. As shown by a recent geochemical study [*Shorttle and Maclennan*, 2011], melting of depleted peridotite is thought to dominate the generation of magma under Iceland. While mantle source heterogeneity is likely to be present, our assumption of a compositionally uniform mantle greatly simplifies the modeling, allowing us to better explore the influence of deglaciation on melting of the dominant mantle lithology under Iceland. Furthermore, the uncertainties on the predicted response of mantle melting to deglaciation resulting from source heterogeneity alone are likely to be insignificant when compared to uncertainties in the mechanical structure.

[27] Significant differences exist between the K03 model and the MB88 and M84-D8 models used by previous studies (Figure 4b). Of these three melt parametrizations, only K03 includes the effect of cpx-out and bulk water content, the latter of these causing reduced melt productivity above the dry solidus and a low melt fraction tail at greater depths (Figure 4a). As pointed out by *Slater et al.* [1998], such a tail is necessary to match the observed geochemistry of late glacial and early postglacial lavas in Iceland. Decreasing T_{pot} from 1500 to 1450°C will shift the initiation of melting upward by 20 and 40 km in a dry model and a model with 620 ppm bulk water, respectively, while the depth of cpx-out is decreased by about 25 km. The melt productivity will therefore be greater at intermediate depths in a cooler model.

[28] The total melting rate can be computed by considering the material derivative of F [*Jull and McKenzie*, 1996]

$$\frac{DF}{Dt} = \left(\frac{\partial F}{\partial P}\right)_S \left(\frac{\partial P}{\partial t} + \overline{\mathbf{V}} \cdot \nabla P\right) \quad (3)$$

where $\partial P/\partial t$ is the in situ pressure change, in this study due to GIA decompression, and $\overline{\mathbf{V}} \cdot \nabla P$ is the pressure change due to upwelling, $\overline{\mathbf{V}}$ being the velocity vector of the solid matrix. Equation (3) allows for a direct comparison of the contribution from the two processes that is independent of the melt productivity equation. Such a comparison, however, can only be done locally as $\partial F/\partial P$ is not constant with depth (Figure 3). For a comparison of total melt volumes generated by upwelling and deglaciation, it is necessary to invoke the full equation which is not independent of $\partial F/\partial P$.

[29] The volume of melt produced at each instant, referred to as melt production rate, Θ, can be estimated by integrating the total melting rate over the melting region, Ω. It is important to note that F is the melt fraction by weight; hence, an integration of equation (3) over the melting volume will not yield a volume [*McKenzie*, 1984]. We therefore

Table 2. Earth Model Parameters Used Within Each Material Layer[a]

Layer	Depth to Base (km)	ρ (kg/m³)	E (GPa)	ν	η (Pa s)
Upper lithosphere	10	2800	65	0.3	∞
Lower lithosphere	35 (mean)	3000	150	0.3	∞
Sublithospheric mantle	∞	3300	210	0.3	10^{19}

[a]ρ—density; E—Young's modulus; ν—Poisson's ratio; η—viscosity. For reference to values listed, see text.

Table 3. Material and Model Parameters Used in the Melting Models[a]

ρ (kg m^{-3})		α (K^{-1})		c_p (J kg^{-1} K^{-1})		Δs	$X_{H_2O}^{bulk}$	M_{cpx}	T_{pot}
solid	melt	solid	melt	solid	melt	(J kg^{-1} K^{-1})	(ppm)	(wt %)	(°C)
3300	2900	4×10^{-5}	6.8×10^{-5}	1200	1500	300	0–620	15	1450–1500

[a]ρ—density; α—thermal expansivity; c_p—specific heat capacity at constant pressure; Δs—specific entropy of fusion; $X_{H_2O}^{bulk}$—bulk water content; M_{cpx}—modal cpx; T_{pot}—potential temperature. See text for references.

first need to convert F to melt fraction by volume, ϕ, yielding the expression

$$\Theta(t) = \int_\Omega \frac{D\phi}{Dt} d\Omega = \int_\Omega \frac{\rho^s \rho^m}{(\rho^m + F(\rho^s - \rho^m))^2} \frac{DF}{Dt} d\Omega \quad (4)$$

From equation (4), we then define the glacially induced melt production rate as

$$\Theta_{GIA} = \int_\Omega \frac{\rho^s \rho^m}{(\rho^m + F(\rho^s - \rho^m))^2} \left(\frac{\partial F}{\partial P}\right)_S \left.\frac{\partial P}{\partial t}\right|_{GIA} d\Omega \quad (5)$$

[30] Neglecting the conversion DF/D$t \to$ Dϕ/Dt before integration results in an underestimation of Θ by up to 20%. We note that neither the study by *Jull and McKenzie* [1996] nor that of *Pagli and Sigmundsson* [2008] used this conversion.

[31] To convert pressures to depths, z, we use the standard expression for lithostatic pressure, $P = \int \rho g dz$, neglecting variations in the gravitational acceleration, g. We further work with potential temperatures as these relate directly to the initial heat budget of the upwelling mantle.

[32] In order to benchmark our implementation, we have successfully reproduced *McKenzie* [1984, Figures 7, 11, and 12] and *Katz et al.* [2003, Figures 2, 3, and 11]. We have also set up the model by *Jull and McKenzie* [1996] and reproduced their results, although in order to do so, we need to assume a gravitational acceleration of 10 m/s^2 and integrate DF/Dt over the assumed melting region rather than Dϕ/Dt.

3.3. Melt Model Parameters

[33] We use the entropy of fusion, densities, and thermal expansion coefficients given by *Katz et al.* [2003] and the heat capacities given by *Bouhifd et al.* [2007], who also measured an entropy of fusion equal to that of *Katz et al.* [2003]. Table 3 summarizes our melt model parameter values.

[34] Compared to the previous studies by *Jull and McKenzie* [1996] and *Pagli and Sigmundsson* [2008], our Δs is slightly smaller (they used 330 J kg^{-1} K^{-1}) while the density of the melt and the heat capacities are larger (they used 2800 kg/m^3 for ρ^m and 1000 J kg^{-1} K^{-1} for both c_p^s and c_p^m). For simplicity, we assume a constant potential temperature beneath Iceland as observations seem to support only minor variations with a preferred value of 1500°C (see section 1.1) [*Maclennan et al.*, 2001; *Kokfelt et al.*, 2003]. However, for a lower bound on our estimates, we also consider a potential temperature of 1450°C. We test bulk water content in the range 0–620 ppm, and we assume a modal cpx of 15 wt %.

4. Mantle Melting Beneath Iceland

[35] Melting of the Icelandic mantle occurs beneath the rift zone as a result of mantle upwelling due to plate spreading and the presence of a hot mantle plume. Here we first define the melting regions where we will investigate glacially induced melting and then we test our melting model and regions with respect to steady state melt production rates.

4.1. Mantle Melting Region

[36] Previous studies of glacially induced melting beneath Iceland have assumed a triangular melting region with a ridge angle, β, of 45° (Figure 5) in agreement with the assumptions of passive upwelling and a ridge perpendicular to the spreading direction. For a 3-D model, however, this assumption is overly simplistic as the rift system in Iceland is neither straight, perpendicular to the spreading direction, nor defined by a single, narrow strand. In addition, as pointed out by *Maclennan et al.* [2002], the assumption of passive upwelling might be inappropriate close to the mantle plume.

[37] In order to specify the melting region and upwelling velocities in a self-consistent way, including upwelling velocities, the full solution to the governing system of equations, including mantle convection, would be necessary. This is beyond the scope of our study. It is, however, reasonable to assume that the melting region widens with depth. We therefore adopt the first-order approximation of a planar boundary between the melting region and the surrounding mantle. We use β to define the slope of the boundary but allow the angle to vary along, as well as on opposite sides of, the rift (Figure 5). The bottom boundary (the solidus) is set by the melt parametrization and model parameters and the top boundary by the base of the elastic layer.

[38] We define one melting region for all of Iceland and also consider two subregions of this. The three melting regions are as follows.

[39] *MR1* (Figure 6a). MR1 is a region beneath the entire Icelandic rift system, representing the melting region due to upwelling. We vary the ridge angle between 45° and 80° in
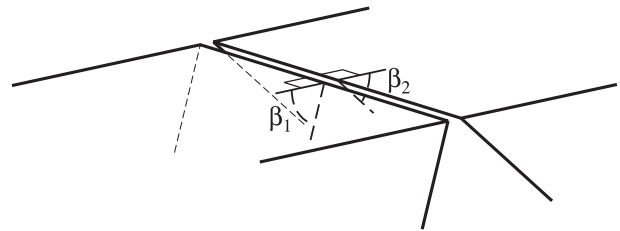

Figure 5. Conceptual model of a spreading ridge with the definition of the ridge angle β, the angle from the surface to the idealized interface between the mantle and the crust, measured perpendicular to the strike of the ridge. The model shows a geometry with different ridge angles, β_1 and β_2, on the left and right sides of the ridge.
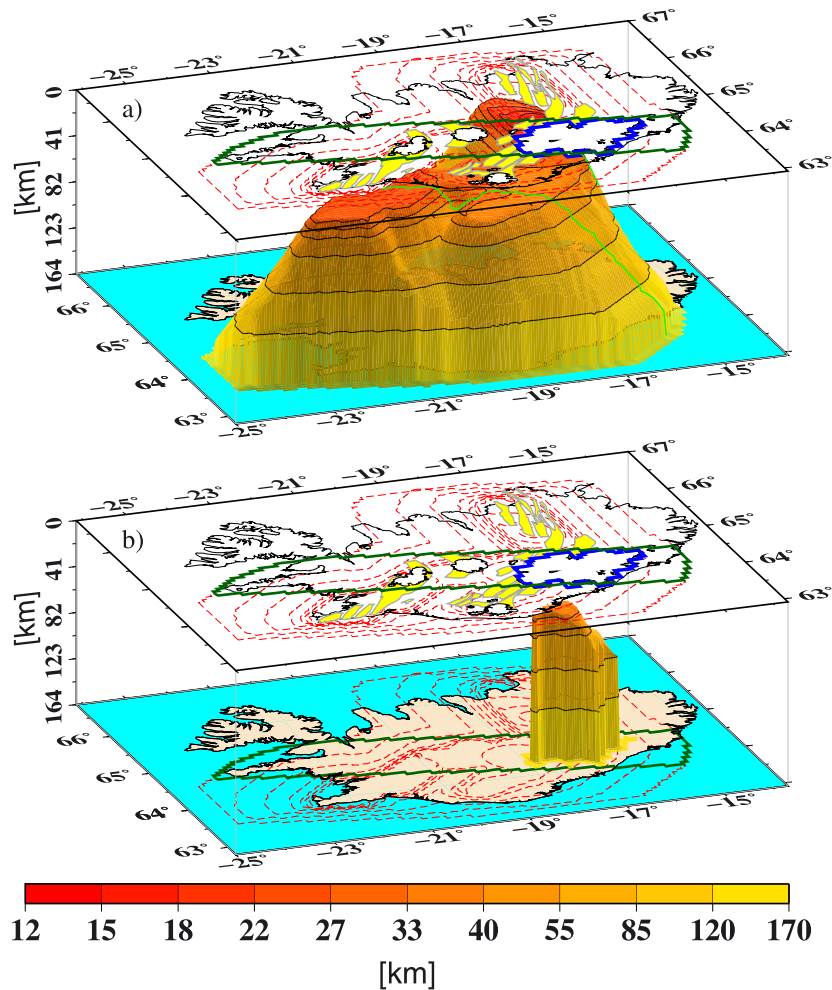
Figure 6. A 3-D view of two of the three modeled melting regions: (a) MR1, the full rift system in Iceland, and (b) MR3, beneath Vatnajökull. The south-southwestern boundary of the strip of MR1 that makes up MR2 is indicated by the thin green line draped onto MR1 in Figure 6a, and the surface projection of MR2 is indicated by the thick dark green polygon in Figures 6a and 6b. The color scale indicates depth, the dashed red contours show the surface projection of MR1, and the thick blue outlined polygon shows the surface projection of MR3. Shorelines and glaciers are outlined with black; the rift zones are indicated by gray polygons and yellow filling.

order to compensate for differences in spreading rate at different sections of the rift and parallel rift segments as well as observations of variations in the lithospheric thickness. The melting region is terminated in the southwest and northeast along lines parallel to the spreading direction and has an approximate length of 420 km from southwest to northeast, measured perpendicular to the spreading direction. We do not extend the melting region along the MAR as the decompression due to deglaciation is small at great distance from the glaciers. We are further mainly interested in melts produced beneath Iceland as these may contribute to the volcanic activity on the island.

[40] *MR2* (Figure 6). MR2 is a 100 km vertical cut of MR1 in central Iceland approximately aligned with the spreading direction and centered beneath the glaciers Hofsjökull, Langjökull, and Vatnajökull, the latter colocated with the most productive Icelandic volcanoes. The region partly coincides with the location of the thickest crust in Iceland (see Figure A1).

[41] *MR3* (Figure 6b). MR3 is a subregion of MR1 located directly beneath Vatnajökull and confined by a vertical cut along the glacier outline. This region is mainly included for a comparison with the earlier study by *Pagli and Sigmundsson* [2008].

[42] In the vicinity of the plume, the mantle ascent velocity may be significantly increased due to buoyancy forces, i.e., active upwelling. The melting region is then expected to be narrower than it would be in the case of passive upwelling. However, we choose not to implement this as geochemical studies combined with variations in the crustal thickness along the ridge imply that active upwelling is significantly reduced above the dry solidus [*Maclennan et al.*, 2001; *Kokfelt et al.*, 2003]. This has also been noted in geodynamical simulations including the effect of dehydration stiffening [*Ito et al.*, 1999; *Ruedas*, 2006], although these studies imposed a viscosity contrast that is not compatible with observations of the present-day GIA in Iceland [*Schmidt et al.*, 2012a].

4.2. Steady State Melt Production Rate

[43] Before we proceed to compute the glacially induced melt production rate, Θ_{GIA}, we evaluate our melt model and the melting regions we have defined. A minimum requirement of the model is that it should generate approximately the correct amount of melt under steady state conditions, i.e., upwelling only, to reproduce the observed crustal thickness in Iceland. We hereafter refer to this as the steady state melt production rate, Θ_{ss}.

[44] Following *Pagli and Sigmundsson* [2008], a minimum estimate of Θ_{ss} can be assessed from the magma volume required to reproduce the mean crustal thickness, h_c, in Iceland:

$$\Theta_{ss} = V_h W h_c \quad (6)$$

where W is the length of the rift system perpendicular to the spreading direction and V_h is the full spreading velocity of the lithosphere across the rift. Crustal thickness in Iceland varies in the range 15–46 km, with a mean value of 20–25 km [e.g., *Darbyshire et al.*, 2000; *Allen et al.*, 2002b; *Fedorova et al.*, 2005; *Bjarnason and Schmeling*, 2009]. Using $V_h \approx 20$ mm/yr, we find a steady state melting rate of 0.17–0.21 km³/yr for the length of MR1.

[45] In central Iceland, the local crustal thickness increases. Assuming a mean crustal thickness of 40 km and a length of the rift section beneath the ice cap of 100 km, the steady state annual melt volume supplying this region, Θ_{ss}^c, is on the order of 0.08 km³/yr.

[46] To compute the steady state melt production rate in our model, $\Theta_{ss,m}$, we first need to know the upwelling velocity in the melting region after which we use equations (3) and (4) to define $\Theta_{ss,m}$:

$$\Theta_{ss,m} = \int_\Omega \frac{\rho^s \rho^m \left(\overline{\mathbf{V}} \cdot \nabla P\right)_{ss}}{(\rho^m + F(\rho^s - \rho^m))^2} \left(\frac{\partial F}{\partial P}\right)_S d\Omega \quad (7)$$

[47] Assuming, for simplicity, that the upwelling velocity $\overline{\mathbf{V}}$ is vertical, V_z, a rough estimate can be obtained from the balance between the upwelling material flux and the lateral material flux. For a triangular cross section of the melting region defined by the ridge angle β and a constant upwelling velocity, this yields the expression

$$\overline{\mathbf{V}} = V_z = V_{xy} \frac{\int \csc(\beta) dW}{\int dW} \quad (8)$$

where V_{xy} is the horizontal velocity of the mantle, dW is a line element along the rift, and csc is the cosecant.

[48] Assuming that the mantle moves horizontally with the same velocity as the lithosphere, $V_{xy} = V_h/2$, we integrate equation (8) over MR1 to yield $V_z = 9.6$ mm/yr. Using this velocity in our melting model, $\Theta_{ss,m}^{MR1} = 0.22$–0.26 km³/yr for a potential temperature of 1500°C and bulk water contents in the range 0–620 ppm. Decreasing T_{pot} to 1450°C reduces the estimate to 0.17–0.20 km³/yr in MR1. Our model is therefore capable of reproducing the observed mean crustal thickness in Iceland. In MR2 and MR3, $\Theta_{ss,m}$ ranges between 0.057 and 0.080 km³/yr and 0.008 and 0.013 km³/yr, respectively, for the range of T_{pot} and $X_{H_2O}^{bulk}$ considered. Hence, melting due to upwelling in MR2 can match the magma volume required to reproduce the crustal thickness in central Iceland.

[49] The assumption of a uniform upwelling rate is not compatible with active upwelling in the plume, and horizontal flow rates are likely to be greater than the spreading

Table 4. Estimated Melt Production Rates due to Present-Day Glacial Unloading in Iceland, Θ_{GIA}[a]

T_{pot} (°C)	$X_{H_2O}^{bulk}$ (ppm)	Θ_{GIA}^{MR3} (km³/yr)	Θ_{GIA}^{MR2}		Θ_{GIA}^{MR1}	
			(km³/yr)	(% Θ_{ss}^c)	(km³/yr)	(% Θ_{ss})
	0	0.044	0.112	140	0.220	105–129
1500	125	0.044	0.113	141	0.226	108–133
	620	0.043	0.112	140	0.229	109–135
	0	0.044	0.113	141	0.206	98–121
1450	125	0.044	0.111	139	0.205	98–121
	620	0.042	0.110	138	0.210	100–124

[a]Estimates are given as a function of bulk water content, $X_{H_2O}^{bulk}$, and potential temperature, T_{pot}, of the mantle. Comparison to estimated steady state melting rates has been included for MR2 and MR1. Material parameters used are given in section 3.3 and Table 3.

velocity in the presence of active upwelling. However, as discussed above, both geochemical studies [*Maclennan et al.*, 2001; *Kokfelt et al.*, 2003] and geodynamic modeling [*Ito et al.*, 1999; *Ruedas*, 2006] indicate that the role of active upwelling is significantly damped above the dry solidus. In addition, equation (6) is based on observations of the mean crustal thickness and therefore sensitive neither to the nature of upwelling beneath Iceland nor to the geometry of the melting region.

5. Glacially Induced Melt Production Rates

[50] The predicted glacially induced melt production rates in our model, Θ_{GIA}, are summarized in Table 4. In MR1, the melting region beneath the entire rift zone across Iceland, the melt production rate induced by deglaciation is approximately 0.21–0.23 km³/yr. Compared to the steady state rate, this corresponds to an increase in the melt production rate by 100–135%. We find that our predictions vary by less than 10% for bulk water contents in the range 0–620 ppm and potential temperatures in the range 1450–1500°C. Approximately half of the melt is generated in MR2 while about 20% of the melt is generated within MR3 (Table 4). Hence, the local increase in the melt production rate in MR3, directly beneath Vatnajökull, is as high as a factor of 4–5.

[51] The sensitivity of Θ_{GIA} to $X_{H_2O}^{bulk}$ and T_{pot} is smaller than the sensitivity of $\Theta_{ss,m}$ to the same parameters. While $\Theta_{ss,m}$ increases by up to 20% when increasing $X_{H_2O}^{bulk}$ from 0 to 620 ppm, Θ_{GIA} will increase by less than 5% in MR1 and decrease slightly in MR2 and MR3. Decreasing the T_{pot} by 50°C lowers the predicted $\Theta_{ss,m}$ by about 30% but Θ_{GIA} only by about 10% in MR1 and almost nothing in MR2 and MR3.

[52] The relatively large response of $\Theta_{ss,m}^{MR1}$ to T_{pot} and $X_{H_2O}^{bulk}$ is due to the assumptions of a constant upwelling velocity in the melting region and a constant density in the mantle. $\Theta_{ss,m}^{MR1}$ will therefore only be dependent on the volume of MR1 and the melt productivity (equation (7)). As the cross section of MR1 is effectively triangular (Figure 6a), its volume will be proportional to $d^2/\tan(\beta)$, where d is the solidus depth. As a result, $\Theta_{ss,m}^{MR1}$ increases with both T_{pot} and $X_{H_2O}^{bulk}$ (Figure 4a). The smaller sensitivity of Θ_{GIA} to these two parameters stems from the nature of the GIA decompression field. Beneath the glaciers, the decompression rate is greatest at shallow depths and decays with increasing depth. Away from the glaciers, the decompression rate increases down to substantial depths before starting to decrease (Figure 3). In

fact, beneath the most remote parts of the rift in Iceland, the highest decompression rate occurs at, or even below, the solidus depth, depending on the water content of the mantle (Figure 4a). Θ_{GIA} will therefore be less sensitive to the solidus depth in regions beneath the glaciers than in regions away from the glaciers. The shallow depth to the maximum decompression rate beneath the glaciers also increases the sensitivity to the depth of cpx-out, which increases with both increasing T_{pot} and $X_{\text{H}_2\text{O}}^{\text{bulk}}$ (Figure 4a). This results in the difference in the trends observed in $\Theta_{\text{GIA}}^{\text{MR1}}$ compared to $\Theta_{\text{GIA}}^{\text{MR3}}$ and $\Theta_{\text{GIA}}^{\text{MR2}}$.

6. Discussion

[53] Our model predictions of glacially induced decompression melting of the Icelandic mantle demonstrate that deglaciation in Iceland since 1890 causes a significant increase in the melt production rate (Table 4). This will most likely affect volcanic activity in Iceland. Our estimates of melt production rates are significantly higher (a factor of 3) than previous studies indicated. Here we will summarize the model assumptions and assess the uncertainties associated with these and with our model parameters. We then compare our results to previous studies and discuss when the glacially induced melt may reach the surface and possible implications for volcanism in Iceland.

6.1. Model Assumptions and Uncertainties

[54] We have modeled the decompression in the mantle using a GIA model with the deglaciation history of Iceland between 1890 and 2010. Of the Earth model parameters, only viscosity and elastic thickness are found to have an effect, albeit small, on melt production rates. Varying these two parameters within ranges permitted by the fit to GPS observations changes our estimated melt production rates beneath the entire rift (MR1; see Table 3) by less than 20%. Although we assume a constant deglaciation rate in the GIA model, the decompression rate changes with time. The melt production rates estimated during the first year after the onset of ice retreat are about 75% of the mean glacially induced melt production rate, while the melt production rates during the last year in our simulation are about 10% higher than the average. Although the actual melt production rate varies from year to year, the total volume produced over time will not be affected. Our estimates presented here are therefore mean melt production rates between 1890 and 2010.

[55] The decompression rates from the GIA model are converted into melt production rates using the melt productivity equation [*McKenzie*, 1984] which is well established and has proven to yield estimates well in agreement with more advanced modeling, solving the full set of governing equations [e.g., *Rudge et al.*, 2011]. Whereas previous studies have chosen melt parametrizations not optimized for the Icelandic mantle, we combine the melt productivity equation with a recent melt parametrization [*Katz et al.*, 2003] appropriate for melting of a depleted peridotite, the dominant mantle lithology under Iceland [*Shorttle and Maclennan*, 2011]. If the mantle contains a more fertile component, such as recycled mid-ocean ridge basalt [*Shorttle and Maclennan*, 2011], more melt would be generated than

predicted by our model. Our choice of parameter values in the melting model (Table 3) increases our estimates by less than 5% compared to the values used in previous studies [*Jull and McKenzie*, 1996; *Pagli and Sigmundsson*, 2008]. We also find that changing the modal cpx by ±5% changes our estimates by ±15–20%.

[56] We select a melting region beneath the entire rift assuming a minor influence of the plume on mantle upwelling above the solidus as indicated by both geochemical studies [*Maclennan et al.*, 2001; *Kokfelt et al.*, 2003] and geodynamic modeling [*Ito et al.*, 1999; *Ruedas*, 2006]. We demonstrate that this melting region is capable of reproducing both the observed mean crustal thickness in Iceland and the locally increased thickness in central Iceland. If active upwelling is occurring to shallow depths, the melting region could be significantly smaller than what we have assumed here, which would decrease our estimates. On the other hand, melting due to glacially induced decompression is not restricted to mantle upwelling regions. Melting will occur everywhere the decompression lowers the solidus temperature below the local mantle temperature. Melts generated outside the upwelling region may, however, not be extracted.

6.2. Comparison to Previous Studies

[57] The only previous study of mantle melting due to deglaciation in Iceland since 1890 is that of *Pagli and Sigmundsson* [2008], which was further discussed in *Sigmundsson et al.* [2010]. *Pagli and Sigmundsson* [2008] considered only deglaciation of Vatnajökull and a melting region directly beneath the ice cap. For a comparison to this study, we have defined a similar melting region, MR3, although it should be stressed that glacially induced melting is not restricted to this region.

[58] Our estimated glacially induced melt production rate in MR3, about 0.044 km^3/yr, is approximately a factor of 3 larger than the estimate by *Pagli and Sigmundsson* [2008] of 0.014 km^3/yr. There are a number of reasons for this. *Pagli and Sigmundsson* [2008] used the M84-D8 melt parametrization suggested by *McKenzie* [1984, equation D8] and assumed a solidus temperature of 1500°C and a solidus depth of 112 km. M84-D8 is, however, a very rough model for mantle melting (see Figure 4) compared to K03 [*Katz et al.*, 2003] used in this study. A solidus temperature of 1500°C is equivalent to a potential temperature of 1416°C, which is lower than our lowest temperature (1450°C). A lower potential temperature will reduce the melt productivity and the volume of the melting region due to a shallower solidus depth. Therefore, the volume of MR3 is about a factor of 1.4 times the volume considered by *Pagli and Sigmundsson* [2008]. Following *Jull and McKenzie* [1996], *Pagli and Sigmundsson* [2008] integrated DF/DP over their melting region instead of Dϕ/DP, causing an underestimation by about 20% as discussed in section 3.2. The study further only considered the deglaciation of Vatnajökull, and while this will yield a higher pressure directly beneath the lithosphere than in our model, the decompression will diminish faster with depth. As Vatnajökull, however, is not centered on top of the rift system, the melting region in *Pagli and Sigmundsson* [2008], as well as MR3 in this study, is offset from the center of Vatnajökull. The largest decompression in the model by *Pagli and Sigmundsson* [2008] therefore occurs outside of their
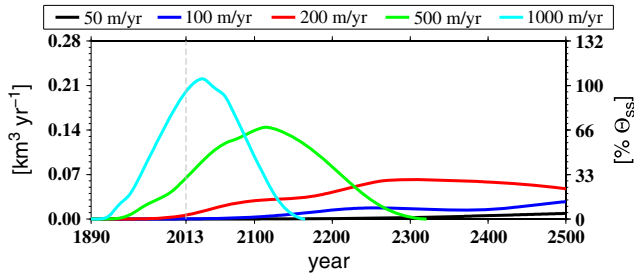
Figure 7. Increase in melt supply rate, ΔMSR, at the base of the elastic lithosphere due to deglaciation of Iceland between 1890 and 2010, assuming a potential temperature of 1500°C, a bulk water content of 125 ppm, and melt ascent velocities of 50 m/yr (black), 100 m/yr (blue), 200 m/yr (red), 500 m/yr (green), and 1000 m/yr (cyan). For percentage of steady state melt production rate, [% Θ_{ss}], 0.21 km³/yr has been used. Note that all curves are based on a time-varying decompression rate between 1890 and 2010, rather than the mean over the period.

melting region. In this study we include deglaciation at other Icelandic glaciers, west of Vatnajökull, which shifts the location of the maximum decompression westward, toward the rift zone and our melting region. These factors explain why we estimate a higher melt production rate than *Pagli and Sigmundsson* [2008]. The melt production rate suggested by *Pagli and Sigmundsson* [2008] is underestimated, but more importantly, the focus on Vatnajökull does not capture the full effect of deglaciation on mantle melting below Iceland.

6.3. Melt Supply Rate at the Base of the Elastic Lithosphere

[59] The additional melt generated by glacially induced decompression will eventually reach the base of the lithosphere, from where it will contribute to the magma supply that feeds intrusive events and volcanic systems in Iceland. The melt supply rate (MSR) at the base of the lithosphere therefore has implications for predictions of increased volcanic activity. Detailed modeling of the melt propagation through the mantle and the lithosphere is beyond the scope of this study. Instead, we use the simple model in *Maclennan et al.* [2002] and consider only the increase in melt supply rate, ΔMSR, at the base of the lithosphere due to deglaciation.

[60] The arrival time, t_L, at the top of the melting column of a package of melt generated at time t_g and depth z_g beneath the base of the lithosphere is estimated from $t_L = t_g + z_g/v_z$, where v_z is the melt ascent velocity. Summing up melt volumes with equal t_L yields ΔMSR. For simplicity, we will assume that v_z is vertical and constant throughout the melting column, although this can be expected to vary with the melting rate, as shown by melt extraction theory [e.g., *McKenzie*, 1984; *Spiegelman*, 1993]. This model nevertheless yields a first-order estimate sufficient for our discussion. Melt ascent velocities as high as 1000 m/yr have been suggested from observations of uranium decay series disequilibrium in Icelandic basalts [e.g., *Stracke et al.*, 2006] as well as the timing of the increased extrusive volumes in Iceland following the end of the last ice age [*Maclennan*

et al., 2002]. We investigate five different v_z in the range 50–1000 m/yr and find that ΔMSR at the base of the lithosphere is highly dependent on v_z. Present-day ΔMSR ranges from negligible to 0.2 km³/yr over the range of v_z considered (Figure 7). This is equivalent to an increase of up to 120% compared to the estimated MSR needed to reproduce the long-term average crustal thickness in Iceland. We also note that none of the ΔMSR curves have reached their peak at present. A sudden increase in melting rates distributed over the entire depth of the melting region will result in a gradual increase in MSR. Only if the increased melting rates are sustained over time periods greater than the longest ascent time through the mantle will ΔMSR be of equal magnitude to the increase in melt production rate. For the case considered here, v_z in excess of 1000 m/yr would be required for the present-day ΔMSR to match the glacially induced melt production rate. For lower velocities, ΔMSR will continue to increase over a time period inversely proportional to the melt ascent velocity, as shown in Figure 7, but it also depends on the future climate and the evolution of the Icelandic glaciers.

6.4. Implications for Extrusive Volumes

[61] An increased MSR at the base of the lithosphere is expected to result in an increase in extrusive volumes at the surface, albeit delayed by the melt migration time through the lithosphere. *Hooper et al.* [2011] found that changing stress conditions in the crust during deglaciation can, in the short term, lead to increased magma capture in the crust outside the ice caps, while beneath the ice caps, an increase in erupted volumes is expected.

[62] The greatest increase in melt production will occur directly beneath Vatnajökull, which covers the most productive Icelandic volcanoes. *Thordarson and Larsen* [2007] estimated that the mean eruption rate in this region throughout the last ~1000 years is about 0.02 km³/yr. Compared to the melt production rates required to reproduce the crustal thickness in central Iceland, about 0.08 km³/yr, this would indicate that about 25% of the melt reaches the surface. Adopting this value as representative for the ratio between eruptive and intrusive events, our maximum estimate of current ΔMSR would correspond to an increase of up to about 0.05 km³/yr in eruption rate spread all along the rift. Approximately half of this volume is predicted to reach the surface in the central 100 km of the rift and at least 20% directly beneath Vatnajökull, feeding the most productive Icelandic volcanoes. A recent large eruption underneath Vatnajökull occurred in Gjálp in 1996 with an estimated volume of about 0.45 km³ of magma [*Gudmundsson et al.*, 2004; *Pagli et al.*, 2007b]. In the more recent 2010 Eyjafjallajökull summit eruption, about 0.18 km³ of magma erupted [*Gudmundsson et al.*, 2012]. Hence, the increase in extrusive volumes in central Iceland could, in the most extreme case considered here, be equivalent to about one Gjálp eruption every 20 years or one Eyjafjallajökull summit eruption about every seventh year.

7. Conclusions

[63] In this study we have examined how the current deglaciation in Iceland affects mantle melting rates. We model glacial isostatic adjustment (GIA) using a finite
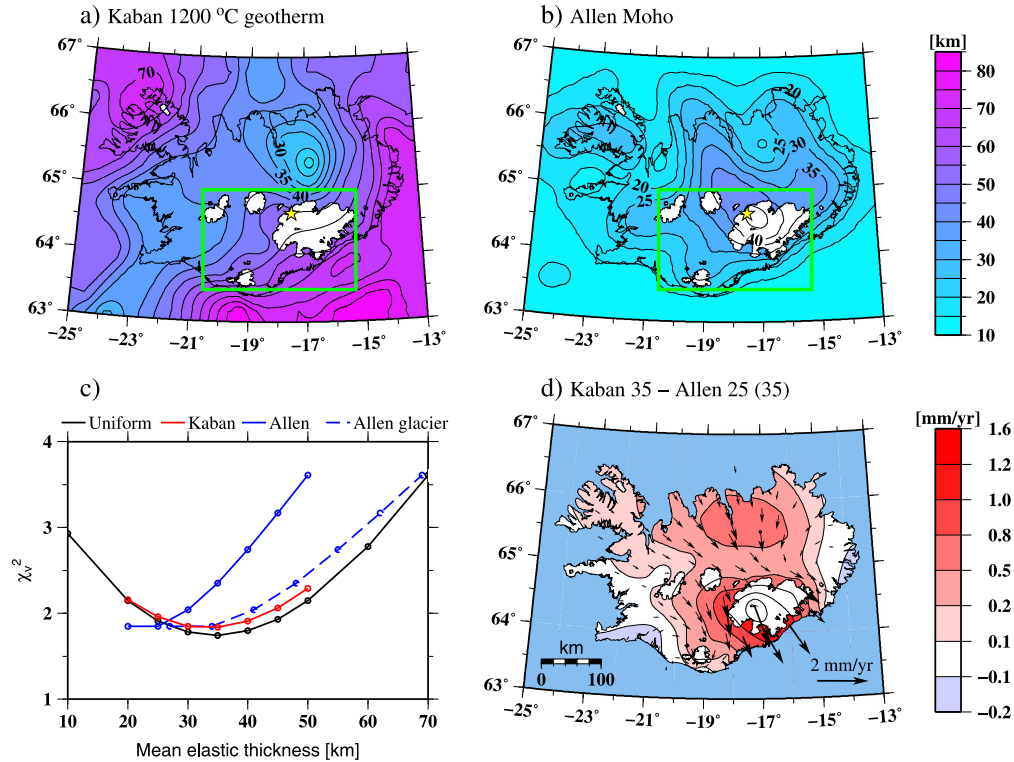
Figure A1. Models with laterally varying elastic thickness of the lithosphere. (a) Depth to the 1200°C isotherm by *Kaban et al.* [2002] (KM). (b) Depth to Moho by *Allen et al.* [2002b] (AM). (c) The χ_v^2 fit to GPS data for models using either KM (red solid line) or AM (blue solid line), as proxies of elastic thickness variations. The proxy models are scaled to mean thicknesses in the range 20–50 km. The blue dashed line shows AM models with mean elastic thickness evaluated over the region outlined by the thick green rectangle in Figures A1a and A1b. The black line shows the fit of a 1-D model with uniform elastic thickness. (d) Difference in predicted deformation rates between KM35 and AM25, the magnitude of the vertical component difference indicated by the color scale. Positive difference indicates higher vertical velocity in KM35. All models assume a mantle viscosity of 10^{19} Pa s. The locations of the major Icelandic glaciers are indicated by regions with white filling. The yellow star in Figures A1a and A1b marks the assumed center of the mantle plume.

element model of the lithosphere and upper mantle, loaded by an ice history model that extends from 1890 to 2010. We find that glacially induced decompression rates in the mantle beneath Iceland vary in both space and time, underlining the need for a proper three-dimensional GIA model. Beneath the ice caps, the decompression rates peak right below the elastic lithosphere, whereas farther away, the maximum decompression rates occur below the onset of melting in the mantle. We estimate that the mean glacially induced melt production rate in the upwelling region is about 0.21–0.23 km³/yr. This is equivalent to an annual melt production increase of 100–135% compared to the background rate. About half of the additional melt is generated beneath central Iceland, while 20% is generated directly beneath the largest ice cap Vatnajökull. We find that the present-day glacially induced increase in melt supply rate, MSR, at the base of the lithosphere ranges from negligible to 0.2 km³/yr, assuming melt ascent velocities in the range 50–1000 m/yr. This is equivalent to up to 120% of the MSR needed for the long-term average crustal production rate in Iceland. If the melt ascent velocity is less than 1000 m/yr, MSR is expected to continue to increase into the future. The increase in MSR is estimated to feed the Icelandic volcanoes

by an additional volume of magma of up to 0.05 km³/yr, where approximately half is produced below central Iceland and 20% concentrated to the region below Vatnajökull, where the most productive Icelandic volcanic systems are located.

Appendix A: The Effect of Laterally Varying Elastic Thickness on GIA in Iceland

[64]   In this study we use the base of the elastic lithosphere as an upper boundary on the melting region beneath Iceland. In order to account for lateral variations of this boundary, we use the depth to the 1200°C isotherm beneath Iceland (Figure A1a) [*Kaban et al.*, 2002] as a proxy for the elastic thickness of the lithosphere. As also the thickness of the Icelandic crust is known to vary laterally (Figure A1b) [e.g., *Darbyshire et al.*, 2000; *Allen et al.*, 2002b; *Fedorova et al.*, 2005; *Bjarnason and Schmeling*, 2009], it is plausible that the GIA process is sensitive to lateral variations in elastic thickness. However, the effect of laterally varying elastic thickness on GIA predictions of surface deformation in Iceland has not been studied so far. We therefore include such a study here.

[65] To study the effect of a laterally varying elastic thickness on the vertical displacement rates, we use both the Moho map by *Allen et al.* [2002b], AM, and the map of the depth to the 1200°C isotherm by *Kaban et al.* [2002], KM. We do not expect any of these to fully describe the mechanically strong lithosphere, represented by the elastic layer in our Earth model. We merely use them as two different proxies. We scale these proxies by constant factors to yield mean elastic thicknesses in the range 20–50 km in steps of 5 km and use a viscosity of 10^{19} Pa s from the best fit 1-D model.

[66] We note a very good correlation between the scaled KM models and the uniform thickness models in the fit to the GPS data as a function of mean elastic thickness, while the AM models suggest a thinner mean elastic thickness (Figure A1c). If, however, the mean thickness is evaluated only over the region enclosing the glaciers included in the ice model (region outlined by the thick green rectangle in Figures A1a and A1b), the mean thickness in the AM models increases by up to 20 km (the blue dashed line in Figure A1c). The same procedure for the KM models changes the mean thickness by less than 1 km and is therefore not shown. Using the adjusted value for the AM models, we see a good correspondence in the data fit of both the AM and KM models to the fit of the 1-D models of equal mean elastic thickness and mantle viscosity. Given the small differences in χ_v^2 seen in Figure A1c, we find that we cannot resolve lateral variations in the elastic thickness on the scales present in the two proxies used.

[67] Figure A1d shows the difference in the predicted deformation rate fields from the best fit AM and KM models. For the KM models, the best fit model has a mean elastic thickness of 35 km, KM35, while for the AM models, the lowest misfit is achieved for a global mean thickness of 25 km, AM25 (mean of 35 km beneath the central glaciers). The KM35 model predicts higher vertical deformation rates in a wide N-S region across Iceland, centered on Vatnajökull (Figure A1d). The difference in the velocities predicted by the two models reaches a magnitude of 1.6 mm/yr beneath central Vatnajökull and exceeds 1 mm/yr along its southern ice edge. The KM model is 0.5–0.8 mm/yr faster than AM25 in a large region north of Vatnajökull. In the horizontal velocities, the difference grows to about 2 mm/yr along the southern edge of Vatnajökull. The sparse number of GPS stations in the regions where the difference is largest explains why the data set we use is insensitive to these lateral variations in the elastic thickness. In addition, we are only using vertical deformation rates as these are least affected by other processes, e.g., plate spreading and magmatic intrusions/extrusions [*Árnadóttir et al.*, 2009]. With more GPS stations closer to the ice edge or possibly InSAR data, especially south of Vatnajökull, or ideally on nunataks, it may be possible to better constrain local variations in the elastic thickness.

References

Albino, F., V. Pinel, and F. Sigmundsson (2010), Influence of surface load variations on eruption likelihood: Application to two Icelandic subglacial volcanoes, Grimsvötn and Katla, *Geophys. J. Int.*, *181*, 1510–1524, doi:10.1111/j.1365-246X.2010.04603.xdoi.

Allen, R. M., et al. (2002a), Imaging the mantle beneath Iceland using integrated seismological techniques, *J. Geophys. Res.*, *107*(B12), 2325, doi:10.1029/2001JB000595.

Allen, R. M., et al. (2002b), Plume-driven plumbing and crustal formation in Iceland, *J. Geophys. Res.*, *107*(B8), 2325, doi:10.1029/2001JB000584.

Árnadóttir, T., S. Jónsson, F. F. Pollitz, W. P. Jiang, and K. L. Feigl (2005), Postseismic deformation following the June 2000 earthquake sequence in the south Iceland seismic zone, *J. Geophys. Res.*, *110*, B12308, doi:10.1029/2005JB003701.

Árnadóttir, T., B. Lund, W. Jiang, H. Geirsson, H. Björnsson, P. Einarsson, and T. Sigurdsson (2009), Glacial rebound and plate spreading: Results from the first countrywide GPS observations in Iceland, *Geophys. J. Int.*, *177*, 691–716, doi:10.1111/j.1365-246X.2008.04059.x.

Asimow, P. D., M. M. Hirschmann, and E. Stolper (1997), An analysis of variations in isentropic melt productivity, *Philos. Trans. R. Soc. London, Ser. A*, *355*, 255–281, doi:10.1098/rtsa.1997.0009.

Auriac, A., K. H. Spaans, F. Sigmundsson, A. Hooper, P. Schmidt, and B. Lund (2013), Iceland rising: Solid Earth response to ice retreat inferred from satellite radar interferometry and viscoelastic modeling, *J. Geophys. Res. Solid Earth*, *118*(4), 1331–1344, doi:10.1002/jgrb.50082.

Bjarnason, I. T., and H. Schmeling (2009), The lithosphere and asthenosphere of the Iceland hotspot from surface waves, *Geophys. J. Int.*, *178*, 394–418, doi:10.1111/j.1365-246X.2009.04155.x.

Björnsson, H. (1979), Glaciers in Iceland, *Jökull*, *29*, 74–80.

Björnsson, H., and F. Pálsson (2008), Icelandic glaciers, *Jökull*, *58*, 365–368.

Bouhifd, M. A., P. Besson, P. Courtial, C. Gérardin, A. Navrotsky, and P. Richet (2007), Thermochemistry and melting properties of basalt, *Contrib. Mineral. Petrol.*, *153*, 689–698, doi:10.1007/s00410-006-0170-8.

Darbyshire, F. A., R. S. White, and K. F. Priestley (2000), Structure of the crust and uppermost mantle of Iceland from a combined seismic and gravity study, *Earth Planet. Sci. Lett.*, *181*, 409–428, doi:10.1016/S0012-821X(00)00206-5.

Delorey, A. A., R. A. Dunn, and J. B. Gaherty (2007), Surface wave tomography of the upper mantle beneath the Reykjanes Ridge with implications for ridge-hot spot interaction, *J. Geophys. Res.*, *112*, B08313, doi:10.1029/2006JB004785.

DeMets, C. G., R. Gordon, D. F. Argus, and S. Stein (1994), Effect of recent revisions to the geomagnetic reversal time scale on estimates of current plate motions, *Geophys. Res. Lett.*, *21*, 2191–2194, doi:10.1029/94GL02118.

Dziewonski, A. M., and D. L. Anderson (1981), Preliminary reference Earth model, *Phys. Earth Planet. Inter.*, *25*, 297–356, doi:10.1016/0031-9201(81)90046-7.

Fedorova, T., W. R. Jacoby, and H. Wallner (2005), Crust-mantle transition and Moho model for Iceland and surroundings from seismic, topography, and gravity data, *Tectonophysics*, *396*, 119–140, doi:10.1016/j.tecto.2004.11.04.

Fleming, K., Z. Martinec, and D. Wolf (2007), Glacial-isostatic adjustment and the viscosity structure underlying the Vatnajökull ice cap, Iceland, *Pure Appl. Geophys.*, *164*, 751–768, doi:10.1007/s00024-007-0187-6.

Gudmundsson, M. T., F. Sigmundsson, H. Bjornsson, and T. Hognadottir (2004), The 1996 eruption at Gjálp, Vatnajokull ice cap, Iceland: Efficiency of heat transfer, ice deformation and subglacial water pressure, *Bull. Volcanol.*, *66*, 46–65, doi:10.1007/s00445-003-0295-9.

Gudmundsson, M. T., et al. (2012), Ash generation and distribution from the April–May 2010 eruption of Eyjafjallajökull, Iceland, *Sci. Rep.*, *2* (572), doi:10.1038/srep00572.

Gudmundsson, O. (2003), The dense root of the Icelandic crust, *Earth Planet. Sci. Lett.*, *206*, 427–440, doi:10.1016/S0012-821X(02)01110-X.

Hardarson, B. S., J. G. Fitton, R. M. Ellam, and M. S. Pringle (1997), Rift relocation—A geochemical and geochronological investigation of a palaeo-rift in northwest Iceland, *Earth Planet. Sci. Lett.*, *157*, 181–196, doi:10.1016/j.epsl.2010.10.010.

Hardarson, B. S., J. G. Fitton, R. M. Ellam, and A. Hjartarson (2008), Tertiary volcanism in Iceland, *Jökull*, *58*, 161–178.

Harðarson, B. S., and G. Fitton (1991), Increased mantle melting beneath Snaefellsjökull volcano during late Pleistocene deglaciation, *Nature*, *353*, 62–64, doi:10.1038/353062a0.

Hirth, G., and D. L. Kohlstedt (1996), Water in the oceanic upper mantle: Implications for rheology, melt extraction and the evolution of the lithosphere, *Earth Planet. Sci. Lett.*, *144*(1–2), 93–108, doi:10.1016/0012-821X(96)00154-9.

Hofton, M. A., and G. R. Foulger (1996), Postrifting anelastic deformation around the spreading plate boundary, north Iceland 1. Modeling of the 1987–1992 deformation field using a viscoelastic Earth structure, *J. Geophys. Res.*, *101*(B11), 25,403–25,421, doi:10.1029/96JB02466.

Hooper, A., B. Ofeigsson, F. Sigmundsson, B. Lund, P. Einarsson, H. Geirsson, and E. Sturkell (2011), Increased capture of magma in the crust promoted by ice-cap retreat in Iceland, *Nat. Geosci.*, *4*, 783–786, doi:10.1038/ngeo1269.

Ito, G., Y. Shen, G. Hirth, and C. J. Wolfe (1999), Mantle flow, melting, and dehydration of the Iceland mantle plume, *Earth Planet. Sci. Lett.*, *165*, 81–96, doi:10.1016/S0012-821X(98)00216-7.

Iwamori, H. (1997), Compression melting in subduction zones, *Terra Nova*, *9*, 9–13, doi:10.1046/j.1365-3121.1997.d01-4.x.

Iwamori, H., D. McKenzie, and E. Takahashi (1995), Melt generation by isentropic mantle upwelling, *Earth Planet. Sci. Lett.*, *134*, 253–266, doi:10.1016/0012-821X(95)00122-S.

Jacoby, W. R., et al. (2009), Temporal gravity variations near shrinking Vatnajökull ice cap, Iceland, *Pure Appl. Geophys.*, *166*, 1283–1302, doi:10.1007/s0024-009-0499-9.

Jamtveit, B., R. Brooker, K. Brooks, L. M. Larsen, and T. Pedersen (2001), The water content of olivines from the North Atlantic Volcanic Province, *Earth Planet. Sci. Lett.*, *186*, 401–415, doi:10.1016/S0012-821X(01)00256-4.

Jull, M., and D. McKenzie (1996), Effect of deglaciation on mantle melting beneath Iceland, *J. Geophys. Res.*, *101*(B10), 21,815–21,828, doi:10.1029/96JB01308.

Kaban, M. K., O. G. Flóvenz, and G. Pálmason (2002), Nature of the crust-mantle transition zone and the thermal state of the upper mantle beneath Iceland from gravity modeling, *Geophys. J. Int.*, *149*, 281–299, doi:10.1046/j.1365-246X.2002.01622.x.

Katz, R. F., M. Spiegelman, and C. H. Langmuir (2003), A new parameterization of hydrous mantle melting, *Geochem. Geophys. Geosyst.*, *4*, 1073, doi:10.1029/2002GC000433.

Kinzler, R. J. (1997), Melting of mantle peridotite at pressures approaching the spinel to garnet transition: Application to mid-ocean ridge basalt petrogenesis, *J. Geophys. Res.*, *102*(B1), 853–874, doi:10.1029/96JB00988.

Kinzler, R. J., and T. L. Grove (1992), Primary magmas of mid-ocean ridge basalts 1. Experiments and methods, *J. Geophys. Res.*, *97*(B5), 6885–6906, doi:10.1029/91JB02840.

Kokfelt, T. F., K. Hoernle, and F. Hauff (2003), Upwelling and melting of the Icelandic plume from radial variation of ^{238}U-^{230}Th disequilibria in postglacial volcanic rocks, *Earth Planet. Sci. Lett.*, *214*(1–2), 167–186, doi:10.1016/S0012-821X(03)00306-6.

LaFemina, P. C., T. H. Dixon, R. Malservisi, T. Árnadóttir, E. Sturkell, F. Sigmundsson, and P. Einarsson (2005), Geodetic GPS measurements in south Iceland: Strain accumulation and partitioning in a propagating ridge system, *J. Geophys. Res.*, *110*, B11405, doi:10.1029/2005JB003675.

Langmuir, C. H., E. M. Klein, and T. Plank (1992), Petrological systematics of mid-ocean ridge basalt: Constraints on melt generation beneath ocean ridges, in *Mantle Flow and Melt Generation, Geophys. Monogr. Ser.,* vol. 71, edited by J. Phipps Morgan, D. Blackman, and J. Sinton, pp. 183–280, AGU, Washington, D.C.

Maclennan, J., D. McKenzie, and K. Gronvöld (2001), Plume-driven upwelling under central Iceland, *Earth Planet. Sci. Lett.*, *194*, 67–82, doi:10.1016/S0012-821X(01)00553-2.

Maclennan, J., M. Jull, D. McKenzie, L. Slater, and K. Gronvöld (2002), The link between volcanism and deglaciation in Iceland, *Geochem. Geophys. Geosyst.*, *3*(11), 1062, doi:10.1029/2001GC000282.

McKenzie, D. (1984), The generation and compaction of partially molten rock, *J. Petrol.*, *25*, 713–765.

McKenzie, D., and M. J. Bickle (1988), The volume and composition of melt generated by extension of the lithosphere, *J. Petrol.*, *29*(3), 625–679.

Nichols, A. R. L., M. R. Carroll, and A. Höskuldsson (2002), Is the Iceland hot spot also wet? Evidence from the water content of undegassed submarine and subglacial pillow basalts, *Earth Planet. Sci. Lett.*, *202*(1), 77–78, doi:10.1016/S0012-821X(02)00758-6.

Pagli, C., and F. Sigmundsson (2008), Will present day glacier retreat increase volcanic activity? Stress induced by recent glacier retreat and its effect on magmatism at the Vatnajökull ice cap, Iceland, *Geophys. Res. Lett.*, *35*, L09304, doi:10.1029/2008GL033510.

Pagli, C., F. Sigmundsson, B. Lund, E. Sturkell, H. Geirsson, P. Einarsson, T. Árnadóttir, and S. Hreinsdóttir (2007a), Glacio-isostatic deformation around the Vatnajökull ice cap, Iceland, induced by recent climate warming: GPS observations and finite element modeling, *J. Geophys. Res.*, *112*, B08405, doi:10.1029/2006JB004421.

Pagli, C., F. Sigmundsson, R. Pedersen, P. Einarsson, T. Arnadottir, and K. L. Feigl (2007b), Crustal deformation associated with the 1996

Gjálp subglacial eruption, Iceland: InSAR studies in affected areas adjacent to the Vatnajokull ice cap, *Earth Planet. Sci. Lett.*, *259*, 24–33, doi:10.1016/j.epsl.2007.04.019.

Pertermann, M., and M. M. Hirschmann (2003), Partial melting experiments on a MORB-like pyroxenite between 2 and 3 GPa: Constraints on the presence of pyroxenite in basalt source regions from solidus location and melting rate, *J. Geophys. Res.*, *108*(B2), 2125, doi:10.1029/2000JB000118.

Phipps Morgan, J. (2001), Thermodynamics of pressure release melting of a veined plum pudding mantle, *Geochem. Geophys. Geosyst.*, *2*(4), 1001, doi:10.1029/2000GC000049.

Pilidou, S., K. Priestley, E. Debayle, and O. Gudmundson (2005), Rayleigh wave tomography in the North Atlantic: High resolution images of the Iceland, Azores and Eifel mantle plumes, *Lithos*, *79*, 453–474, doi:10.1016/j.lithos.2004.09.012.

Pollitz, F. F., and I. S. Sacks (1996), Viscosity structure beneath northeast Iceland, *J. Geophys. Res.*, *101*(B8), 17,771–17,793, doi:10.1029/96JB01074.

Rudge, J. F., D. Bercovici, and M. Spiegelman (2011), Disequilibrium melting of a two phase multicomponent mantle, *Geophys. J. Int.*, *184*, 699–718, doi:10.1111/j.1365-246X.2010.04870.x.

Ruedas, T. (2006), Dynamics, crustal thicknesses, seismic anomalies, and electrical conductivities in dry and hydrous ridge-centered plumes, *Phys. Earth Planet. Inter.*, *155*, 16–41, doi:10.1016/j.pepi.2005.09.007.

Ruedas, T., H. Schmeling, and G. Marquart (2007), Iceland: The current picture of a ridge-centered mantle plume, in *Mantle Plumes—A Multidisciplinary Approach*, edited by U. R. Christensen, pp. 71–126, Springer-verlag, Berlin, Heidelberg.

Sæmundsson, K. (1967), An outline of the structure of SW-Iceland, in *Iceland and Mid-Ocean Ridges*, edited by S. Björnsson, pp. 151–161, Rit 38, Soc. Sci. Islandica, Reykjavik, Iceland.

Schmidt, P., B. Lund, T. Árnadóttir, and H. Schmeling (2012a), Effects of dehydration stiffening in the mantle constrained by glacial rebound in Iceland, *Earth Planet. Sci. Lett.*, *359–360*, 152–161, doi:10.1016/j.epsl.2012.10.015.

Schmidt, P., B. Lund, and C. Hieronymus (2012b), Implementation of the glacial rebound pre-stress advection correction in general-purpose finite element analysis software: Springs versus foundations, *Comp. Geosci.*, *40*, 97–106, doi:10.1016/j.cageo.2011.07.017.

Shorttle, O., and J. Maclennan (2011), Compositional trends of Icelandic basalts: Implications for short-length scale lithological heterogeneity in mantle plumes, *Geochem. Geophys. Geosyst.*, *12*, Q11008, doi:10.1029/2011GC003748.

Sigmundsson, F., and P. Einarsson (1992), Glacio-isostatic crustal movements caused by historical volume change of the Vatnajökull ice cap, Iceland, *Geophys. Res. Lett.*, *19*, 2123–2126, doi:10.1029/92GL02209.

Sigmundsson, F., V. Pinel, B. Lund, A. Fabien, C. Pagli, H. Geirsson, and E. Sturkell (2010), Climate effects on volcanism: Influence on magmatic systems of loading and unloading from ice mass variations, with examples from Iceland, *Philos. Trans. R. Soc. London, Ser. A*, *368*, 2519–2534, doi:10.1098/rsta2010.0042.

Sigvaldason, G. E., K. Annertz, and M. Nilsson (1992), Effect of glacier loading/deloading on volcanism: Postglacial volcanic production rate of the Dyngjufjöll area, central Iceland, *Bull. Volcanol.*, *54*, 385–392, doi:10.1007/BF00312320.

Sinton, J., K. Grönvold, and K. Sæmundsson (2005), Postglacial eruptive history of the Western Volcanic Zone, Iceland, *Geochem. Geophys. Geosyst.*, *6*, Q12009, doi:10.1029/2005GC001021.

Slater, L., M. Jull, D. McKenzie, and K. Gronvöld (1998), Deglaciation effects on mantle melting under Iceland: Results from the Northern Volcanic Zone, *Earth Planet. Sci. Lett.*, *164*, 151–164, doi:10.1016/S0012-821X(98)00200-3.

Spiegelman, M. (1993), Physics of melt extraction: Theory, implications and applications, *Philos. Trans. R. Soc. London, Ser. A*, *342*(1663), 23–41, doi:10.1098/rsta.1993.0002.

Stracke, A., B. Bourdon, and D. McKenzie (2006), Melt extraction in the Earth's mantle: Constraints from U-Th-Pa-Ra studies in oceanic basalts, *Earth Planet. Sci. Lett.*, *244*, 97–112, doi:10.1016/j.epsl.2006.01.057.

Thórarinsson, S. (1943), Oscillations of the Iceland glaciers in the last 250 years, *Geog. Ann.*, *25*, 1–54.

Thordarson, T., and G. Larsen (2007), Volcanism in Iceland in historical time: Volcano types, eruption styles and eruptive history, *J. Geodyn.*, *43*, 118–152, doi:10.1016/j.jog.2006.09.005.

Wessel, P., and W. H. F. Smith (1991), Free software helps map and display data, *EOS Trans. AGU*, *72*, 441–446, doi:10.1029/90EO00319.

Wu, P. (2004), Using commercial finite element packages for the study of earth deformations, sea levels and the state of stress, *Geophys. J. Int.*, *158*, 401–408, doi:10.1111/j.1365-246X.2004.02338.x.